Orbital Degeneracy Removed by Charge Order in Triangular Antiferromagnet $AgNiO_2$

E. Wawrzyńska,[1] R. Coldea,[1] E. M. Wheeler,[2,3] I. I. Mazin,[4] M. D. Johannes,[4] T. Sörgel,[5] M. Jansen,[5] R. M. Ibberson,[6] and P. G. Radaelli[6]

[1]*H. H. Wills Physics Laboratory, University of Bristol, Tyndall Avenue, Bristol BS8 1TL, United Kingdom*
[2]*Clarendon Laboratory, University of Oxford, Parks Road, Oxford OX1 3PU, United Kingdom*
[3]*Institute Laue-Langevin, B.P. 156, 38042 Grenoble Cedex 9, France*
[4]*Code 6393, Naval Research Laboratory, Washington, D.C. 20375, USA*
[5]*Max-Planck Institut für Festkörperforschung, Heisenbergstrasse 1, D-70569 Stuttgart, Germany*
[6]*ISIS Facility, Rutherford Appleton Laboratory, Chilton, Didcot OX11 0QX, United Kingdom*

(Received 4 May 2007; published 11 October 2007)

We report a high-resolution neutron diffraction study on the orbitally degenerate spin-1/2 hexagonal metallic antiferromagnet $AgNiO_2$. A structural transition to a tripled unit cell with expanded and contracted NiO_6 octahedra indicates $\sqrt{3} \times \sqrt{3}$ charge order on the Ni triangular lattice. This suggests charge order as a possible mechanism of lifting the orbital degeneracy in the presence of charge fluctuations, as an alternative to the more usual Jahn-Teller distortions. A novel magnetic ground state is observed at low temperatures with the electron-rich $S = 1$ Ni sites arranged in alternating ferromagnetic rows on a triangular lattice, surrounded by a honeycomb network of nonmagnetic and metallic Ni ions. We also report first-principles band-structure calculations that explain microscopically the origin of these phenomena.

DOI: 10.1103/PhysRevLett.99.157204 PACS numbers: 75.25.+z, 61.12.Ld, 71.45.Lr, 75.50.Ee

Electronic systems on triangular lattices have attracted wide interest theoretically and experimentally due to the possible existence of unconventional ground states stabilized by the frustrated lattice geometry [1]. The layered cobaltate $NaCoO_2$ with a triangular lattice of orbitally *nondegenerate* Co^{3+} ions [2] shows a number of unusual phases upon hole doping via deintercalation of Na, as well as superconductivity upon hydration at a particular doping [1]. The addition of orbital degeneracy creates more instabilities for cooperative order, and the behavior in the presence of metallic conductivity is not well understood and largely experimentally unexplored. In more localized systems such as $NaNiO_2$ with spin-1/2 Ni^{3+} ions in the $t_{2g}^6 e_g^1$ configuration, the twofold e_g orbital degeneracy is lifted by a Jahn-Teller (JT) structural distortion to a monoclinic structure [3], which splits the e_g band and opens a gap. However, it is unclear if such a mechanism applies in less localized systems where the local tendency for JT distortions competes with the charge transfer between sites, allowed by an efficient metallic screening [4]. The metallic layered silver nickelates $AgNiO_2$ [5,6] and Ag_2NiO_2 [7] are ideal candidates to explore this physics.

Here we report high-resolution structural studies of $AgNiO_2$ and find that no JT distortions occur but the ideal structure is distorted to a *hexagonal tripled* unit cell with expanded and contracted NiO_2 octahedra. This implies that the orbital degeneracy of the formally Ni^{3+} sites is lifted by a novel $\sqrt{3} \times \sqrt{3}$ charge ordering (CO) that occurs via the charge transfer $3e_g^1 \rightarrow e_g^2 + e_g^{0.5} + e_g^{0.5}$, which to the best of our knowledge is the first experimental example of such a CO pattern in a triangular system. Using band-structure calculations, we show that this CO is a 2D analogue of the metal-insulator transition in the 3D $RNiO_3$ [8] attributed to the charge transfer $2e_g^1 \rightarrow e_g^2 + e_g^0$ [4]. However, in contrast to the 3D nickelates in $AgNiO_2$, the triangular lattice geometry allows the system to remain metallic in the CO phase, as itinerant electrons can hop on the interconnected honeycomb network formed by the two electron-depleted sublattices ($e_g^{0.5}$); those sites remain magnetically unordered at base temperature. The remaining one-third of Ni sites are strongly magnetic (e_g^2) and form an effectively tripled antiferromagnetic (AFM) triangular lattice, which orders in an unusual collinear 2×1 structure of alternating stripes.

Powder samples of $2H$-$AgNiO_2$ (a polymorph [5] of the better known rhombohedral $3R$ polytype [6]) were prepared as described in Ref. [5], and neutron diffraction indicates a nearly pure hexagonal phase with less than 1% admixture of the rhombohedral polytype. Neutron diffraction patterns at 300 K were collected using the high-resolution time-of-flight diffractometers OSIRIS and HRPD at the ISIS pulsed neutron source, and representative results are shown in Fig. 1(a), yielding the hexagonal space group $P6_3/mmc$ as proposed earlier [5], with triangular Ni, O, and Ag layers stacked as *ABBBA* (Ni-O-Ag-O-Ni). However, the neutron data show additional diffraction peaks [see Figs. 1(b)–1(d)] which can be consistently indexed by an ordering wave vector $\boldsymbol{k}_0 = (1/3, 1/3, 0)$ in the original undistorted structure, indicating a tripled unit cell in the hexagonal plane. To test the accuracy of the indexing, we have refined the lattice parameters using only the main peaks and only the supercell peaks (more than 20 observed) and obtained the same values to within the experimental accuracy of 10^{-4} Å. Furthermore, upon cooling to 2 K, the supercell peaks were displaced in Q following the lattice contraction but maintained their commensurate index with respect to the main peaks. This further confirms that the supercell peaks are due to a modu-

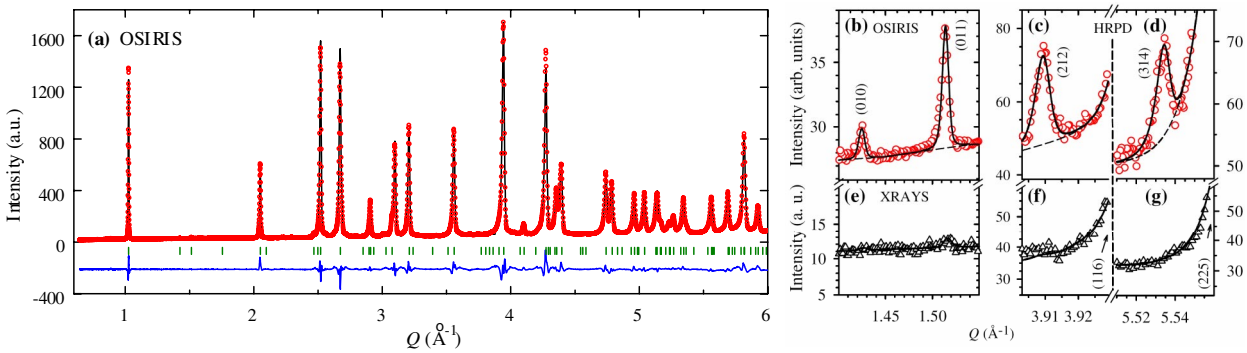

FIG. 1 (color online). (a) 300 K neutron powder diffraction pattern and (b)–(d) zoomed-in regions showing some of the prominent supercell peaks which indicate a distortion of the high-symmetry $P6_3/mmc$ structure where all Ni sites are equivalent. (e)–(g) Supercell peaks are not observed in x-ray data, indicating that the distortion involves mainly displacements of oxygen ions. Solid lines in all panels are fits to the model with periodic arrangement of expanded and contracted NiO_6 octahedra shown in Fig. 2, and peak indexing is in the triple unit cell (space group $P6_322$).

lation of the main structure rather than an extra impurity phase.

X-ray data collected using a Phillips Cu K_α powder diffractometer [Figs. 1(e)–1(g)] do not show supercell peaks, indicating that the distortion involves mainly the light oxygen ions. Thus, we refined the neutron data in a $\sqrt{3} \times \sqrt{3}$ hexagonal unit cell assuming only oxygen displacements. We eliminated the space groups that were not compatible with the observed low-temperature magnetic structure (to be described later), dictating at least two different Ni crystallographic sites. The highest symmetry space group in which both the structural and magnetic data could be described is $P6_322$ (no. 182). Good agreement with the data is obtained (solid line fits [9] in Fig. 1), and the extracted unit cell parameters are listed in Table I. As a further check of the space group identification, we have performed full structural optimization calculations (as described later) starting from a lower symmetry structure ($P6_3$ space group), and those invariably converged to the higher $P6_322$ symmetry, with the optimized positions agreeing well with the experimental ones (Table I) [10].

The resulting structure in one NiO_2 layer is shown in Fig. 2. There are three inequivalent Ni sites. Oxygens breathe in towards Ni2 and Ni3 ions ($d_{\text{Ni2-O}} = d_{\text{Ni3-O}} = 1.934$ Å) and out from Ni1 ($d_{\text{Ni1-O}} = 2.022$ Å). No Jahn-Teller distortion is present. The different Ni-O distances indicate that Ni1 is electron-rich (Ni^{2+} in a CO scenario) and Ni2,3 are electron-depleted ($Ni^{3.5+}$). In the adjacent NiO_2 layer, Ni1 and Ni3 sites swap places, leading to a zigzag arrangement of the (expanded) electron-rich Ni1 sites along c [11].

Earlier susceptibility data [5] showed dominant antiferromagnetic couplings with a Curie-Weiss constant $\theta = -107.6$ K and AFM order below $T_N = 22$ K. Below this temperature, additional peaks appear in the neutron diffraction pattern; see Fig. 3(a). These peaks are indexed by the ordering wave vector $\boldsymbol{k} = (1/2, 0, 0)$, as shown in the inset in Fig. 3(a). The best fit was obtained when only one Ni sublattice was ordered, either Ni1 or Ni3, with a moment of $1.522(7)\mu_B$ along the c axis. As discussed above,

TABLE I. Unit cell lattice parameters in the ideal ($P6_3/mmc$) and CO ($P6_322$) structures at 300 K. Internal parameters δ, ζ, ξ, and ϵ are 0, 0.08050(5), 0, and 0.0133(2) (exp.) and 0, 0.0792, 0, and 0.0102 (calc.), respectively.

$P6_3/mmc$ (no. 194)			$P6_322$ (no. 182)		
$a_0 = 2.93919(5)$ Å			$a = 5.0908(1)$ Å		
$c = 12.2498(1)$ Å			$c = 12.2498(1)$ Å		
Atom	Site	(x, y, z)	Atom	Site	(x, y, z)
Ni	$2a$	$(0, 0, 0)$	Ni1	$2c$	$(\frac{1}{3}, \frac{2}{3}, \frac{1}{4})$
			Ni2	$2b$	$(0, 0, \frac{1}{4})$
			Ni3	$2d$	$(\frac{1}{3}, \frac{2}{3}, \frac{3}{4})$
Ag	$2c$	$(\frac{2}{3}, \frac{1}{3}, \frac{1}{4})$	Ag	$6g$	$(\frac{2}{3} + \delta, 0, 0)$
O	$4f$	$(\frac{2}{3}, \frac{1}{3}, \zeta)$	O	$12i$	$(\frac{1}{3} + \xi, \epsilon, \frac{1}{4} + \zeta)$

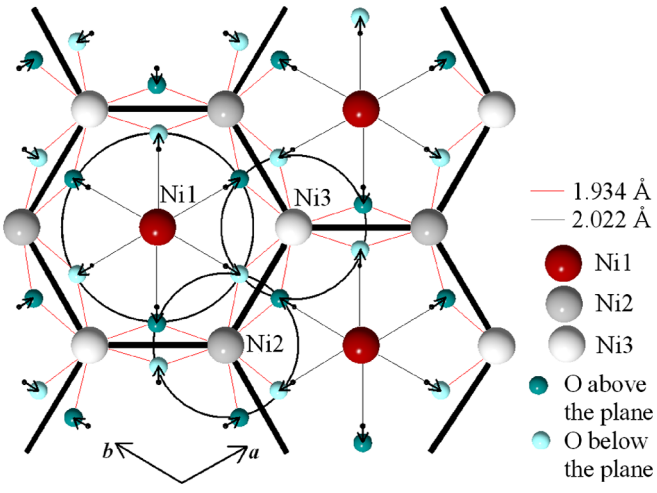

FIG. 2 (color online). Bottom NiO_2 layer showing the expanded $Ni1O_6$ octahedra (large circle) surrounded by a honeycomb network (thick lines) of contracted Ni2 and Ni3 sites (small circles). The small balls are oxygen ions, and the small arrows indicate the displacements from the ideal structure.

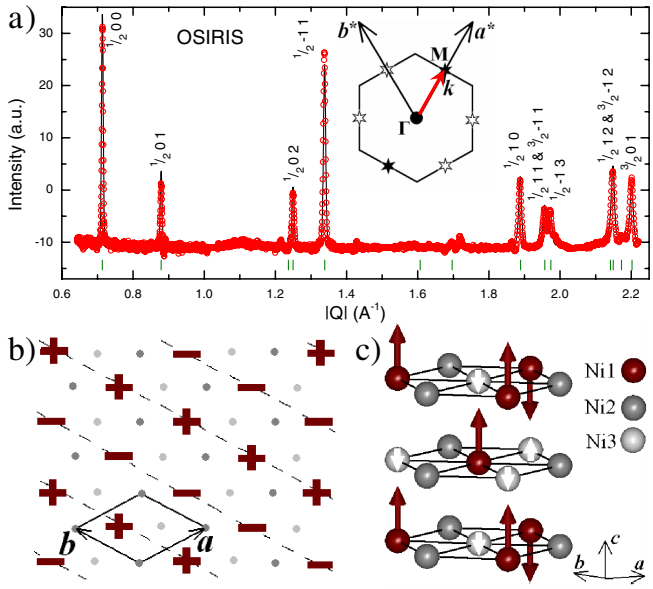

FIG. 3 (color online). (a) Magnetic diffraction pattern (difference 4–300 K) indexed by wave vector $\boldsymbol{k} = (1/2, 0, 0)$. The solid line is a fit to the spin order depicted in (b). In one layer, ordered spins (Ni1) form alternating ferromagnetic rows, $\pm$ symbols indicate spin projection along the c axis, and gray balls are unordered sites (Ni2 and Ni3). The diamond-shaped box is the unit cell. (c) 3D view of the magnetic order along the c axis. Band-structure calculations indicate that the effective FM interlayer coupling between the strongly magnetic Ni1 spins (large arrows) occurs via AFM couplings to a very small moment at the Ni3 site (small white arrow). The inset in (a) shows the 2D hexagonal Brillouin zone with locations of magnetic Bragg peaks [solid stars for the stripe domain in (b), open stars for equivalent domains rotated by $\pm 60°$].

this must be the strongly magnetic Ni1 (Ni^{2+}) with a large available moment of $S = 1$ ($2\mu_B$), because Ni3 and Ni2 are $Ni^{3.5+}$ with only a small available moment.

The observed magnetic structure is shown in Fig. 3(b): In each layer, ordered spins are arranged in alternating FM stripes; in the adjacent layer, stripes are parallel but have an in-plane offset that follows the c-axis zigzag arrangement of the electron-rich Ni1 sites; see Fig. 3(c). This magnetic structure implies that (a) the exchange between nearest in-plane magnetic neighbors is AFM, (b) there is an easy-axis anisotropy $-DS_z^2$, and (c) the net interplanar interaction with the 3 magnetic neighbors in the layer above (below) [see Fig. 3(c)] is FM.

To gain more insight into the physical origin for the observed charge and magnetic orderings, we have performed density functional (DFT) calculations [12,13]. Since Ag_xNiO_2 is metallic and only weakly correlated [14], introducing a Hubbard U in the calculation is not necessary. Optimizing the oxygen positions in the $\sqrt{3} \times \sqrt{3}$ unit cell precipitates the CO and reproduces the observed structure in Fig. 2, indicating that the driving force for charge disproportionation is entirely accounted for in the local-density approximation. The calculated total magnetization for the three Ni ions varies between 1.3 and $1.5\mu_B$, depending on the exact O position, and is nearly entirely located at the expanded Ni1 site in good quantitative accord with the neutron data. The computed ferromagnetic band structure (Fig. 4) shows fully exchange-split Ni1 derived bands with the magnetic moment diminished from its formal count of $2\mu_B$ by hybridization. One can also see that Ni2 and Ni3 states are not visibly exchange-split. The Ag sp band is entirely above the Fermi level. This electronic structure can be visualized as a magnetic insulator formed by Ni^{2+} (cf. NiO) with a strong tendency to magnetic order, superimposed on a $Ni^{3.5}$ metal. The latter has larger bandwidths, due to the smaller Ni-O distance, and by itself does not satisfy the Stoner criterion for metallic magnetism $IN(E_F) > 1$, where I is the atomic Stoner parameter.

The natural tendency for charge order in a NiO_2 layer can be explained by energetic arguments. The Hund's rule energy gain in a metal in DFT is $M^2(I - N^{-1})/4$, where N is the average density of states per spin. Without charge ordering, $M_1 = M_2 = M_3 = 1\mu_B$ and $N_1 = N_2 = N_3 = \bar{N}$. After charge ordering, $M_1 \approx 2\mu_B$, $M_2 = M_3 \approx 0$, and $N_1 > \bar{N} > N_2 = N_3$. The CO state is energetically favored since $4(I - N_1^{-1})/4 > 3(I - \bar{N}^{-1})/4$. In insulators such as $NaNiO_2$, the Hubbard repulsion would forbid this mechanism, but in this metallic system it is well screened and cannot prevent CO [15]. Our band-structure calculations reproduce fully the observed 3D CO pattern, both the in-plane $\sqrt{3} \times \sqrt{3}$ order as well as the zigzag arrangement of the electron-rich sites along c. We also found a metastable solution where the CO layers form straight columns along c: i.e., the electron-rich and strongly magnetic Ni^{2+} occupy the Ni2 site; this indicates that the in-plane CO is very robust and independent of the interlayer magnetic interactions.

To study the stability of the observed magnetic structure, we have calculated ground state energies for a number of

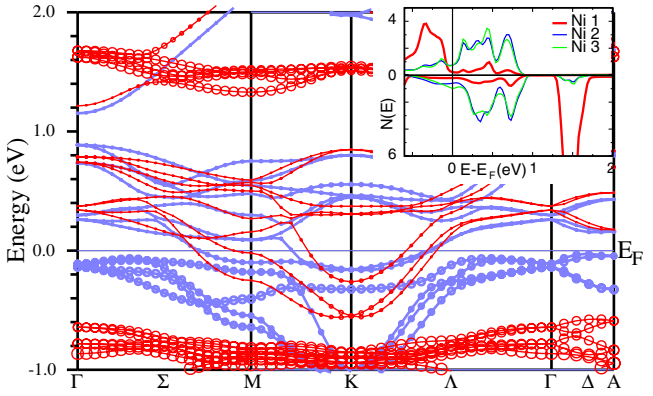

FIG. 4 (color online). Ferromagnetic band structure of $2H$-$AgNiO_2$ along symmetry directions in the Brillouin zone. Blue/red (light/dark) correspond to the up/down spin directions, and circles indicate the relative weight of the Ni1 states. Inset: Partial densities of states for the three Ni sites in states/eV/triple cell. Top/bottom: Spin majority (up)/minority (down).

TABLE II. Energies of different magnetic configurations for $2H$-$AgNiO_2$. All energies are expressed per magnetic Ni1 ion and as a difference from the calculated (and observed) magnetic ground state.

	Stripe-F	Stripe-A	FM	A-type AFM
Energy/Ni1 (meV)	0	7	23	21

potential structures using DFT for the full magnetic unit cell (12 f.u. and lower symmetry, C2). In addition to the observed stripe order with the zigzag ferromagnetic pattern along c shown in Figs. 3(b) and 3(c) (called stripe-F), we also found stable solutions for hypothetical FM, A-type AFM (alternating FM layers), as well as in-plane stripe order but with a zigzag AFM pattern along c (stripe-A, every other plane flipped compared to stripe-F). The results are listed in Table II; the state found experimentally has the lowest energy.

The magnetic structure indicates that the in-plane exchange between magnetic neighbors is AFM. This arises naturally because $Ni1^{2+}$ sites are insulating and lack both metallic Stoner ferromagnetism and 90° FM superexchange but do have a classical AFM superexchange via the Ni1-O-O-Ni1 path, with effective hopping $t_{\text{eff}} \sim t_{pd\sigma}^2 t_{pp\pi}/(E_d - E_p)^2$. The appearance of collinear order instead of the conventional 120° order for a triangular AFM implies a significant easy-axis anisotropy. This is normally provided by spin-orbit-induced coupling to the crystal field, but the Ni1 ion is close to a $t_{2g}^6 e_g^2$ configuration with zero orbital moment. Further experimental and theoretical studies of the single-site anisotropy in this system are under way. The fact that the effective interplanar Ni1-Ni1 exchange is FM is rather surprising, since there is *a priori* no apparent physical mechanism for FM couplings. Indeed, the magnetic species Ni1 forms insulating bands, and Ag is nonmagnetic and absent from the Fermi energy, eliminating double exchange as a possibility. Ni2 and Ni3 form quasi-2D bands with small potential for sizable RKKY interaction, and magnetic impurities in the Ag layer that could mediate a FM exchange have been excluded experimentally.

Performing calculations for a wider range of parameters, we find that, depending on the exact positions of Ag and O, the interplanar interaction can change amplitude and even sign and that an effective FM interlayer coupling appears if the weakly magnetic site Ni3 has a small ordered moment (0.10–$0.15\mu_B$). The strongest interplanar interaction is AFM superexchange between the Ni3 and Ni1 directly above (it occurs via a nearly collinear O-Ag-O path), whereas the interplanar Ni1-Ni1 exchange is much weaker. If the Ni3 moment is aligned antiparallel to the Ni1 above it, then the structure in Fig. 3(c) has a net energy gain as it also satisfies two out of the three in-plane AFM Ni3-Ni1 couplings. Our diffraction data in Fig. 3(a) cannot prove or exclude the existence of very small moments on Ni3, but the data is consistent with a Ni3 moment of $\sim 0.1\mu_B$ antialigned with the Ni1 directly above it, as it comes out of the calculations.

To summarize, we have reported high-resolution neutron diffraction in the orbitally degenerate $2H$-$AgNiO_2$. We observe a periodic arrangement of expanded and contracted NiO_6 octahedra, naturally explained by a three-sublattice charge order pattern on the triangular lattice of Ni sites. We have proposed that, due to Hund's rule coupling and metallic screening of the Hubbard U repulsion (and static screening due to oxygen displacements), the CO is the favored mechanism to lift the orbital degeneracy as opposed to the conventional Jahn-Teller distortions that occur in more insulating systems. An unusual magnetic order is observed at low temperatures with only one-third of sites carrying a magnetic moment with an unexpected collinear stripe-order pattern on an antiferromagnetic triangular lattice. Our results indicate the complex cooperative charge and magnetic order patterns that can occur in orbitally degenerate metallic systems on frustrated lattices.

We acknowledge support from EPSRC UK.

[1] N. P. Ong and R. J. Cava, Science **305**, 52 (2004).
[2] M. Jansen and R. Hoppe, Z. Anorg. Allg. Chem. **408**, 104 (1974).
[3] E. Chappel *et al.*, Eur. Phys. J. B **17**, 615 (2000).
[4] I. I. Mazin *et al.*, Phys. Rev. Lett. **98**, 176406 (2007).
[5] T. Sörgel and M. Jansen, Z. Anorg. Allg. Chem. **631**, 2970 (2005); J. Solid State Chem. **180**, 8 (2007).
[6] Y. J. Shin *et al.*, J. Solid State Chem. **107**, 303 (1993).
[7] M. Schreyer and M. Jansen, Angew. Chem. **41**, 643 (2002); U. Wedig *et al.*, Solid State Sci. **8**, 753 (2006); H. Yoshida *et al.*, Phys. Rev. B **73**, 020408(R) (2006).
[8] J. A. Alonso *et al.*, Phys. Rev. Lett. **82**, 3871 (1999).
[9] J. Rodríguez-Carvajal, Physica (Amsterdam) **192B**, 55 (1993).
[10] Experimentally, the Ni1-O bond is 4.5% longer than the other two Ni-O bonds; the calculations find 3.5%. The optimized position of O is mainly insensitive to the position of Ag ions. The Ag ions (located between two O's in the high-symmetry structure) do not follow the O ions upon the breathing distortion, remaining instead in a practically ideal triangular lattice. These facts indicate that CO is an intrinsic instability of the NiO_2 layer which is only loosely bound to the close-packed Ag layer.
[11] Prominent supercell peaks [Figs. 1(b) and 1(c)] such as (011) and (212) rule out an arrangement where the expanded Ni sites are directly above each other in adjacent layers.
[12] P. Blaha *et al.*, *WIEN2K* (Technische Universität Wien, Austria, 2001).
[13] G. Kresse and J. Furthmuller, Phys. Rev. B **54**, 11 169 (1996).
[14] M. D. Johannes *et al.*, Phys. Rev. B **75**, 180404 (2007).
[15] This analysis does not take into account increase on the Ni-O covalent energy that also favors charge ordering [W. A. Harrison, Phys. Rev. B **74**, 245128 (2006)].